PTEP

Prog. Theor. Exp. Phys. **2021**, 083I01 (17 pages)
DOI: 10.1093/ptep/ptab074

Muon spin motion at the crossover regime between Gaussian and Lorentzian distribution of magnetic fields

Muhamad Darwis Umar[1,2], Katsuhiko Ishida[1], Rie Murayama[1], Dita Puspita Sari[1,3], Utami Widyaiswari[1,4], Marco Fronzi[3], Harion Rozak[1,5,6], Wan Nurfadhilah Zaharim[1,5,6], Isao Watanabe[1,2,4,5,6,*], and Masahiko Iwasaki[†,1]

[1]*RIKEN, Hirosawa 2-1, Wako-shi, Saitama 351-0198, Japan*
[2]*Hokkaido University, Kita 10 Nishi 8, Sapporo, 060-0810, Japan*
[3]*Shibaura Institute of Technology, 307 Fukasaku, Minuma, Saitama 337-8570, Japan*
[4]*Universitas Indonesia, Depok 16424, Indonesia*
[5]*Universiti Sains Malaysia, Pulau Pinang 11800, Malaysia*
[6]*USM-RIKEN International Centre for Advanced Sciences, Universiti Sains Malaysia, Pulau Pinang 11800, Malaysia*
*E-mail: nabedon@riken.jp
†These authors contributed equally to this work.

Received May 1, 2021; Revised June 8, 2021; Accepted June 8, 2021; Published August 2, 2021

The muon spin relaxation method is a powerful microscopic tool for probing the electronic states of materials by observing local magnetic field distributions on the muon. It often happens that a distribution of local magnetic fields shows an intermediate state between Gaussian and Lorentzian shapes. In order to generally describe these intermediate field distributions, we considered the convolution of two isotropic distributions in three dimensions and derived exact muon-spin relaxation functions which can be applied to all crossover regimes between Gaussian and Lorentzian.

Subject Index I42, I43, I46, I47

1. Introduction

The muon spin relaxation (μSR) technique is a powerful microscopic probe for investigating the electronic states of materials from the atomic viewpoint. After a muon is injected into the target material, keeping the self-spin polarization along the injection trajectory, the muon decays to a positron with a lifetime of 2.2 μs while interacting with the surrounding electronic states [1]. The asymmetric emission of positrons along the muon spin direction is detected by forward and backward counters and the time dependence of the muon spin polarization (μSR time spectrum) is measured. By analyzing the μSR time spectrum we can investigate magnetic transitions [2–10], superconducting states [11–15], molecular motions [16], electronic orbital states [17,18], ionic/spin diffusions [19–24], and so on. Since the muon is injected from outside the material, μSR can be widely applied to many kinds of materials.

The choice of analysis functions is a key matter in deducing physics information from the μSR results in order to understand the changes in electronic states in various temperature regions. For instance, local magnetic fields at the muon site in the paramagnetic state are well known to arise from

© The Author(s) 2021. Published by Oxford University Press on behalf of the Physical Society of Japan.
This is an Open Access article distributed under the terms of the Creative Commons Attribution License (http://creativecommons.org/licenses/by/4.0/), which permits unrestricted reuse, distribution, and reproduction in any medium, provided the original work is properly cited.

Downloaded from https://academic.oup.com/ptep/article/2021/8/083I01/6335693 by University of Technology, Sydney user on 11 February 2022

surrounding nuclear dipole moments, resulting in the formation of a Gaussian field distribution at the muon site. The Gaussian distribution typically occurs when there are independent contributions from many magnetic sources with similar contributions. Simple metals like Cu are good examples of this situation. The local field observed at the muon site in Cu is produced by nuclear dipole moments of Cu surrounding the muon and satisfies the conditions for realizing the Gaussian distribution [25,26]. In this case, the μSR time spectrum is well described by the Gaussian Kubo–Toyabe (GKT) function, $P_{\mathrm{GKT}}(t)$ [27,28]:

$$P_{\mathrm{GKT}}(t) = \frac{1}{3} + \frac{2}{3}(1 - \Delta^2 t^2) \exp\left(- \frac{\Delta^2 t^2}{2} \right). \tag{1}$$

Here, Δ is the half width of the Gaussian distribution of the magnetic field at the muon site. This GKT-type relaxation behavior of the μSR time spectrum is observed in the paramagnetic state of many kinds of materials [25,26,29,30].

The Lorentzian distribution tends to occur when contributions from a single magnetic source dominate. One typical example is a dilute spin-glass system. In this case, one magnetic spin, which is located nearest to the muon, tends to give a dominant contribution [26]. In those low-density spin systems, the local field due to the random and sparse magnetic dipole has an axial magnetic field distribution proportional to $B^2/(a^2 + \gamma_\mu^2 B^2)^2$ for the dilute limit (effectively for concentrations less than 3%–5%), called the Lorentzian field [31]. B is the distributed magnetic field with half width a, and γ_μ is the muon's gyromagnetic ratio ($\gamma_\mu = 2\pi \times 135.5\,\mathrm{MHz\,T^{-1}}$). This situation is described by the Lorentzian Kubo–Toyabe (LKT) function, $P_{\mathrm{LKT}}(t)$ [26]:

$$P_{\mathrm{LKT}}(t) = \frac{1}{3} + \frac{2}{3}(1 - at) \exp(-at). \tag{2}$$

An intermediate μSR time spectrum can be considered as a crossover distribution, with characteristics somewhere between Gaussian and Lorentzian. For instance, in the case that there are two independent field contributions, one with a Gaussian distribution and the other Lorentzian, an intermediate local field distribution can be realized. Another possible case is when the source is from a single magnetic origin but the number of contributing magnetic spins is small, though not one.

Recently, another way to realize an intermediate μSR time spectrum was reported for systems with non-uniform and/or low-density distributions of nuclear magnetic moments. Organic molecular superconductors are typical examples showing this kind of distribution [32–34]. Such systems have low-dimensional crystal structures and low-density alignments of nuclear magnetic moments, resulting in deformation of the Gaussian distribution of magnetic fields.

When a magnetic transition appears with decreasing temperatures, an intermediate μSR time spectrum is frequently observed around the magnetic transition temperatures for a different reason. Near the magnetic transition temperature, additional internal fields coming from surrounding fluctuating electronic magnetic moments appear at the muon site. These additional fields are a couple of orders larger than those coming from nuclear magnetic moments. When approaching the magnetic transition temperature, fluctuating electronic magnetic fields become mandatory and the μSR time spectrum changes from Gaussian to Lorentzian, reflecting the spin–spin correlation function [15,26,30,35–37]. Some examples showing such changes in the time spectrum were reported in the La-based high-T_c superconducting oxide $La_{2-x}Sr_xCuO_4$, especially in the underdoped regime [36,37].

Downloaded from https://academic.oup.com/ptep/article/2021/8/083I01/6335693 by University of Technology, Sydney user on 11 February 2022

In such cases, phenomenological functions have been used to analyze the intermediate time spectra. One example is

$$e^{-\lambda t} \times P_{\mathrm{GKT}}(t), \tag{3}$$

where λ is regarded as the dynamic relaxation rate of the muon spin polarization caused by fluctuating electronic spins. This phenomenological function is used on the basis of the assumption that the measured system contains localized electronic moments which are fluctuating in time. However, the two parameters sometimes cause a trading-off effect in describing the intermediate time spectrum, resulting in failures to reveal realistic electronic states.

The stretched Kubo–Toyabe (SKT) function is also a well-used analysis function [38]:

$$P_{\mathrm{SKT}}(t) = \frac{1}{3} + \frac{2}{3}(1 - (\lambda t)^{\alpha}) \exp(-(\lambda t)^{\alpha}/\alpha)). \tag{4}$$

Here, α ($\alpha = 1$–2) and λ are the stretch parameter and the relaxation rate of the muon spin polarization, respectively. $P_{\mathrm{SKT}}(t)$ matches $P_{\mathrm{LKT}}(t)$ at $\alpha = 1$ and $P_{\mathrm{GKT}}(t)$ at $\alpha = 2$. Although this form has been widely used for many μSR results because of the ease of programming the fit, it is difficult to get physical ideas of how α and λ can be related to the actual field distribution and the spin dynamics.

Therefore, it is important to describe the intermediate muon spin relaxation function in order to study crossover phenomena under the coexistence of two random and static (in the time range of muon spin precession) magnetic fields which are independent of each other. Until now, various analysis functions have been developed to describe the μSR time spectrum; however, intermediate μSR time spectra have not yet been described successfully enough. Phenomenological equations that mix Gaussian and Lorentzian functions have been examined [39,40], and one generalized theoretical function was suggested for the analysis of the intermediate state [41]. These recent suggestions prove the high interest in developing an analysis function for the intermediate μSR time spectrum, and this requirement is increasing year by year.

For the current study, we describe the crossover field in terms of a convoluted function of Gaussian and Lorentzian distributions. We derive the equation of the three-dimensional (3D) convolution in two ways. The first derivation uses the convolution integral starting directly in 3D space. The other derivation starts from the one-dimensional (1D) convolution integral and converts it to the 3D form. From the latter, we show that the equation can be decomposed into a sum of three known convolutions. By applying the Fourier transform to this equation we achieve the correct relaxation function for the zero-field condition, which was found to be given by a simple analytical equation. In addition, we try to describe the intermediate analysis function under applied magnetic fields and under dynamic fluctuations on the basis of the development of the zero-field intermediate analysis function. Finally, we apply our developed analysis function to some μSR results in order to ensure its validity.

2. Field distribution and relaxation function under coexistence of Gaussian and Lorentzian distributions

2.1. Conversion between 3D and 1D magnetic field distributions

We start by showing how the 1D and 3D distributions of magnetic fields can be related when the field direction is random (namely, isotropic). First, we define the probability of finding a site with the magnetic field $\boldsymbol{B} = (B_x, B_y, B_z)$ as $\rho_3(\boldsymbol{B})d^3\boldsymbol{B}$ (see Fig. 1). If the field distribution is isotropic, with $\rho_3(\boldsymbol{B})$ having no dependence on the direction, we may write $\rho_3(\boldsymbol{B})d^3\boldsymbol{B} = \rho_3(B)B^2 dB d(\cos\theta) d\phi$,

Downloaded from https://academic.oup.com/ptep/article/2021/8/083I01/6335693 by University of Technology, Sydney user on 11 February 2022

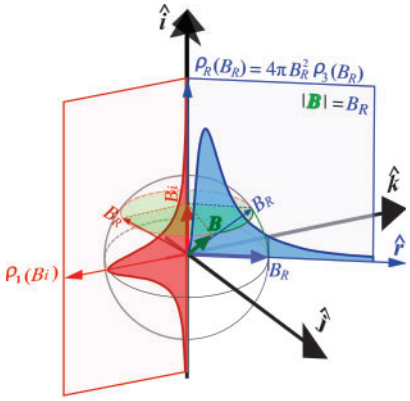

Fig. 1. Relation between the 3D field distribution, $\rho_3(\boldsymbol{B})$, and its distribution projection in one dimension, $\rho_1(B_i)$. We also define the field size distribution, $\rho_R(B)$. They are normalized so that $\int_{-\infty}^{+\infty} \rho_1(B_i)dB_i = 1$, $4\pi \int_0^{+\infty} \rho_3(B)B^2 dB = 1$, and $\int_0^{+\infty} \rho_R(B)dB = 1$.

where B is the size of the local field. We also define the distribution of the field size as $\rho_R(B)dB$; then $\rho_R(B) = 4\pi B^2 \rho_3(B)$. The distribution of the field component in one direction, for example B_z, is given by $\rho_1(B_z)dB_z$. In the cylindrical coordinated (B_z, B_ρ, ϕ), we get, by projection,

$$\rho_1(B_z) = \int_0^\infty \rho_3(B) 2\pi B_\rho dB_\rho, \tag{5}$$

where $B^2 = B_z^2 + B_\rho^2$ and the integration is done keeping B_z constant. Using $BdB = B_\rho dB_\rho$,

$$\rho_1(B_z) = \int_{B_z}^\infty \rho_3(B) 2\pi B dB. \tag{6}$$

It follows that

$$d\rho_1(B_z)/dB_z = -2\pi B_z \rho_3(B_z). \tag{7}$$

As the expression of the variable does not matter, we rewrite Eq. (7) as

$$\rho_3(B) = -(1/2\pi B) d\rho_1(B)/dB, \tag{8}$$

and

$$\rho_R(B) = -2B d\rho_1(B)/dB. \tag{9}$$

We set two distributions of B, Gaussian and Lorentzian. Each distribution is characterized by Δ or a as the width of the distribution. For Gaussian, we get

$$\rho_{1,\mathrm{G}}(B) = (\gamma_\mu/\sqrt{2\pi}\Delta) \exp(-\gamma_\mu^2 B^2/2\Delta^2), \tag{10}$$

$$\rho_{3,\mathrm{G}}(B) = (\gamma_\mu^3/(2\pi)^{3/2}\Delta^3) \exp(-\gamma_\mu^2 B^2/2\Delta^2), \tag{11}$$

$$\rho_{R,\mathrm{G}}(B) = (2^{1/2}\gamma_\mu^3/\pi^{1/2}\Delta^3) B^2 \exp(-\gamma_\mu^2 B^2/2\Delta^2). \tag{12}$$

For the Lorentzian case,

$$\rho_{1,\mathrm{L}}(B) = (\gamma_\mu/\pi) a/(a^2 + \gamma_\mu^2 B^2), \tag{13}$$

Downloaded from https://academic.oup.com/ptep/article/2021/8/083I01/6335693 by University of Technology, Sydney user on 11 February 2022

$$\rho_{3,\mathrm{L}}(B) = (\gamma_\mu^3/\pi^2)a/(a^2+\gamma_\mu^2 B^2)^2, \tag{14}$$

$$\rho_{R,\mathrm{L}}(B) = (4\gamma_\mu^3/\pi)aB^2/(a^2+\gamma_\mu^2 B^2)^2. \tag{15}$$

2.2. *Three-dimensional convolution of the static magnetic field distribution*

First, we describe the distribution $\rho_{\mathrm{GL}}(B)$ as the convolution of the Gaussian and Lorentzian fields. For the distribution of the summed field component in one direction we can use 1D convolution,

$$\begin{aligned}\rho_{1,\mathrm{GL}}(B) &= \int dB_1 \rho_{1,\mathrm{G}}(B-B_1)\rho_{1,\mathrm{L}}(B_1) \\ &= (a\gamma_\mu^2/\sqrt{2}\pi^{3/2}\Delta)\int dB_1 \exp(-\gamma_\mu^2(B-b_1)^2/2\Delta^2)/(a^2+\gamma_\mu^2 B^2).\end{aligned} \tag{16}$$

To obtain the 3D distribution $\rho_3(\boldsymbol{B})$ of the vector summed field, we need 3D convolution. The convolution should be done by varying one of the fields, $\boldsymbol{B}_1$, while the other field is automatically determined. This leads to $\boldsymbol{B}_2 = \boldsymbol{B} - \boldsymbol{B}_1$. The probability of having $\boldsymbol{B}_1$ and $\boldsymbol{B}_2$ at the same time is $\rho_{3,\mathrm{G}}(\boldsymbol{B}_2)\rho_{3,\mathrm{L}}(\boldsymbol{B}_1)$. This probability should be integrated for all possible $\boldsymbol{B}_1$ to find the probability of having field $\boldsymbol{B}$. Thus,

$$\begin{aligned}\rho_{3,\mathrm{GL}}(\boldsymbol{B}) &= \int d^3\boldsymbol{B}_1 \rho_{3,\mathrm{G}}(\boldsymbol{B}_2)\rho_{3,\mathrm{L}}(\boldsymbol{B}_1) \\ &= 2\pi\int\int B_1^2 dB_1 d(\cos\theta_1)\rho_{3,\mathrm{G}}(B_2)\rho_{3,\mathrm{L}}(B_1) \\ &= (\gamma_\mu^3/(2\pi)^{3/2}\Delta^3)(a\gamma_\mu^3/\pi^2)\int\int dB_1 d(\cos\theta_1)\exp(-\gamma_\mu^2 B_2^2/2\Delta^2)B_1^2/(a^2+\gamma_\mu^2 B_1^2)^2,\end{aligned} \tag{17}$$

where $B_2^2 = B^2 + B_1^2 - 2B_1 B\cos\theta_1$. The integration over $\cos\theta_1$ can be done analytically, giving

$$\begin{aligned}\rho_{3,\mathrm{GL}}(B) &= (\sqrt{2}a\gamma_\mu^4/\pi^{3/2}\Delta)\int_0^{+\infty} dB_1 B B_1 \\ &\quad\times[\exp(-\gamma_\mu^2(B-B_1)^2/2\Delta^2) - \exp(-\gamma_\mu^2(B+B_1)^2/2\Delta^2)]/(a^2+\gamma_\mu^2 B_1^2)^2 \\ &= (\sqrt{2}a\gamma_\mu^4/\pi^{3/2}\Delta)\int_{-\infty}^{+\infty} dB_1 B B_1 \exp(-\gamma_\mu^2(B-B_1)/2\Delta^2)/(a^2+\gamma_\mu^2 B_1^2)^2.\end{aligned} \tag{18}$$

Next, we show another derivation of the 3D convolution form. When two independent distributions contribute, the projected sum of fields is represented by the 1D convolution,

$$\rho_{1,\mathrm{GL}}(B) = \int_{-\infty}^{+\infty} dB_1 \rho_{1,\mathrm{G}}(B-B_1)\rho_{1,\mathrm{L}}(B_1). \tag{19}$$

As the sum of field distribution is also isotropic, using the relation in Eq. (9) we get

$$\begin{aligned}\rho_{R,\mathrm{GL}}(B) &= -2Bd\rho_{1,\mathrm{GL}}(B)/dB \\ &= \int dB_1(-2B)(d\rho_{1,\mathrm{G}}(B-B_1)/dB)\rho_{1,\mathrm{L}}(B_1).\end{aligned} \tag{20}$$

It can be shown that this leads to the same form as Eq. (18). However, instead, we here derive another form, applying the Fourier transform to obtain the relaxation function

$$\rho_{R,\mathrm{GL}}(B) = \int dB_1(-2(B-B_1)-2B_1)(d\rho_{1,\mathrm{G}}(B-B_1)/dB)\rho_{1,\mathrm{L}}(B_1) \tag{21}$$

Downloaded from https://academic.oup.com/ptep/article/2021/8/083I01/6335693 by University of Technology, Sydney user on 11 February 2022

from the relations $-2(B-B_1)d\rho_{1,\mathrm{G}}(B-B_1)/dB = \rho_{R,\mathrm{G}}(B-B_1)$ and $d\rho_{1,\mathrm{G}}(B-B_1)/dB = -d\rho_{1,\mathrm{G}}(B-B_1)/dB_1$,

$$\begin{aligned}
\rho_{R,\mathrm{GL}}(B) &= \int_{-\infty}^{+\infty} dB_1 \rho_{R,\mathrm{G}}(B-B_1)\rho_{1,\mathrm{L}}(B_1) + \int_{-\infty}^{+\infty} dB_1 (d\rho_{1,\mathrm{G}}(B-B_1)/dB_1) 2B_1\rho_{1,\mathrm{L}}(B_1) \\
&= \int_{-\infty}^{+\infty} dB_1 \rho_{R,\mathrm{G}}(B-B_1)\rho_{1,\mathrm{L}}(B_1) + [\rho_{1,\mathrm{G}}(B-B_1)2B_1\rho_{1,\mathrm{L}}(B_1)]_{-\infty}^{+\infty} \\
&\quad - \int_{-\infty}^{+\infty} dB_1 \rho_{1,\mathrm{G}}(B-B_1) d(2B_1\rho_{1,\mathrm{L}}(B_1))/dB_1 \\
&= \int_{-\infty}^{+\infty} dB_1 \rho_{R,\mathrm{G}}(B-B_1)\rho_{1,\mathrm{L}}(B_1) - \int_{-\infty}^{+\infty} dB_1 \rho_{1,G}(B-B_1)(2B_1 d\rho_{1,L}(B_1)/dB_1) \\
&\quad - \int_{-\infty}^{+\infty} dB_1 \rho_{1,\mathrm{G}}(B-B_1) 2\rho_{1,\mathrm{L}}(B_1) \\
&= \int_{-\infty}^{+\infty} dB_1 \rho_{R,\mathrm{G}}(B-B_1)\rho_{1,\mathrm{L}}(B_1) + \int_{-\infty}^{+\infty} dB_1 \rho_{1,\mathrm{G}}(B-B_1)\rho_{R,\mathrm{L}}(B_1) \\
&\quad - 2\int_{-\infty}^{+\infty} dB_1 \rho_{1,\mathrm{G}}(B-B_1)\rho_{1,\mathrm{L}}(B_1). \qquad (22)
\end{aligned}$$

As the above manipulation is purely mathematical, we should note that the ρ_R are defined even in the negative B range by Eq. (9), and $\rho_R(-B) = \rho_R(B)$ as the $\rho_1(B)$ are assumed symmetric.

2.3. Muon spin relaxation function under isotropic field distribution

Now, let's discuss muon spin in reference to the internal field distribution $\rho_R(B)$. Hence, muons have a polarization axis as an ensemble, and the polarization can be depolarized (relaxed) in time due to spin precession around the internal field, because each muon will sense a different magnetic field at its particular position. For simplicity, we describe this in a semi-classical manner. An example of muon spin precession is illustrated schematically in Fig. 2. Taking the quantum axis to be in the direction of the muon polarization at $t = 0$, θ and ϕ are the polar and azimuthal angles of B at the muon site, respectively. B is distributed randomly in angle with reference to the quantum axis. Its field strength is described by the 3D distribution $\rho_3(B)$ (or the size distribution $\rho_R(B)$). The muon spin precesses around B with the Larmor precession frequency, ω_μ, where $\omega_\mu = \gamma_\mu B$. By taking the ensemble, the component vertical to the initial polarization is canceled out because of the symmetry, so only the spin polarization parallel to the initial spin remains:

$$\begin{aligned}
P(t) &= \int\int\int d^3\boldsymbol{B}[\cos^2\theta + \sin^2\theta\cos(\gamma_\mu Bt)]\rho_3(B) \\
&= \int dB \int d(\cos\theta)[\cos^2\theta + \sin^2\theta\cos(\gamma_\mu Bt)]\frac{1}{2}\rho_R(B). \qquad (23)
\end{aligned}$$

In the case of an isotropic field distribution $\rho_R(B)$ is independent of θ, so the we can take an integral over $\cos\theta$, resulting in

$$P(t) = \frac{1}{3} + \frac{2}{3}\int_0^\infty \cos(\gamma_\mu Bt)\rho_R(B)dB = \frac{1}{3} + \frac{2}{3}P_{\mathrm{osc}}(t), \qquad (24)$$

Downloaded from https://academic.oup.com/ptep/article/2021/8/083I01/6335693 by University of Technology, Sydney user on 11 February 2022

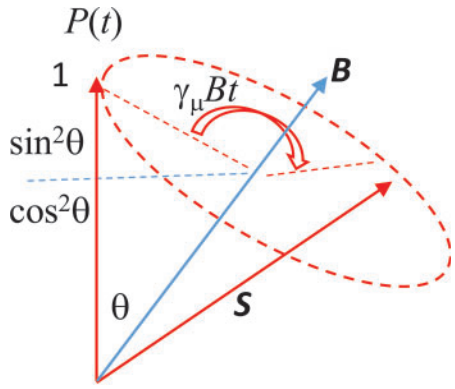

Fig. 2. The spin rotation in a zero field. The decomposition of the muon polarization into the spin-conserving part, $\cos^2\theta$, and the spin-precession part, $\sin^2\theta$, is shown. The precession part rotates around the internal magnetic field $\boldsymbol{B}$ with the Larmor frequency of $\gamma_\mu B$.

where $P_{\rm osc}(t)$ is the oscillation component of the muon spin relaxation. We now define two Fourier transforms, one in the range 0 to $+\infty$ and the other in the range $-\infty$ to $+\infty$:

$$\hat{\rho}^+(t) = \int_0^{+\infty} \cos(\gamma_\mu B t)\rho(B)dB, \qquad \hat{\rho}(t) = \int_{-\infty}^{+\infty} \cos(\gamma_\mu B t)\rho(B)dB. \tag{25}$$

For a symmetric distribution $\rho(B)$, $\hat{\rho}(t) = 2\hat{\rho}^+(t)$.

Now we set $P_{\rm osc}(t) = \hat{\rho}^+_{R,\rm GL}(t)$, where the field distribution is given as the convolution in Eq. (22):

$$\begin{aligned}
\hat{\rho}^+_{R,\rm GL}(t) &= \frac{1}{2}\hat{\rho}_{R,\rm GL}(t) \\
&= \frac{1}{2}\int_{-\infty}^{\infty} \cos(\gamma_\mu B t)\rho_{R,\rm GL}(B)dB \\
&= \frac{1}{2}\int_{-\infty}^{\infty} \cos(\gamma_\mu B t)\left[\int_{-\infty}^{+\infty} dB_1 \rho_{R,\rm G}(B-B_1)\rho_{1,\rm L}(B_1)\right]dB \\
&\quad + \frac{1}{2}\int_{-\infty}^{\infty} \cos(\gamma_\mu B t)\left[\int_{-\infty}^{+\infty} dB_1 \rho_{1,\rm G}(B-B_1)\rho_{R,\rm L}(B_1)\right]dB \\
&\quad - \int_{-\infty}^{\infty} \cos(\gamma_\mu B t)\left[\int_{-\infty}^{+\infty} dB_1 \rho_{1,\rm G}(B-B_1)\rho_{1,\rm L}(B_1)\right]dB.
\end{aligned} \tag{26}$$

Using well-known features of the Fourier transform of functions f and g, the additive principle ($\widehat{f+g} = \hat{f} + \hat{g}$) and the convolution principle ($\widehat{f * g} = \hat{f} \times \hat{g}$), where $f * g$ means convolution,

$$\begin{aligned}
\hat{\rho}^+_{R,\rm GL}(t) &= \frac{1}{2}\int_{-\infty}^{\infty} \cos(\gamma_\mu B t)\rho_{R,\rm G}(B)dB \int_{-\infty}^{+\infty} \cos(\gamma_\mu B t)\rho_{1,L}(B)dB \\
&\quad + \frac{1}{2}\int_{-\infty}^{\infty} \cos(\gamma_\mu B t)\rho_{1,\rm G}(B)dB \int_{-\infty}^{+\infty} \cos(\gamma_\mu B t)\rho_{R,\rm L}(B)dB \\
&\quad - \int_{-\infty}^{\infty} \cos(\gamma_\mu B t)\rho_{1,\rm G}(B)dB \int_{-\infty}^{+\infty} \cos(\gamma_\mu B t)\rho_{1,\rm L}(B)dB \\
&= \frac{1}{2}\hat{\rho}_{R,\rm G}(t)\hat{\rho}_{1,\rm L}(t) + \frac{1}{2}\hat{\rho}_{1,\rm G}(t)\hat{\rho}_{R,\rm L}(t) - \hat{\rho}_{1,\rm G}(t)\hat{\rho}_{1,\rm L}(t) \\
&= \hat{\rho}^+_{R,\rm G}(t)\hat{\rho}_{1,\rm L}(t) + \hat{\rho}_{1,\rm G}(t)\hat{\rho}^+_{R,\rm L}(t) - \hat{\rho}_{1,\rm G}(t)\hat{\rho}_{1,\rm L}(t).
\end{aligned} \tag{27}$$

Downloaded from https://academic.oup.com/ptep/article/2021/8/083I01/6335693 by University of Technology, Sydney user on 11 February 2022

Note that this relation is applicable as far as the two distributions are independent and both isotropic. In the special case when the two distributions are Gaussian and Lorentzian their Fourier counterparts are well-known, including those for 3D distributions [25,27,28]:

$$\hat{\rho}_{1,\mathrm{G}}(t) = \exp(-\Delta^2 t^2/2) \tag{28}$$

$$\hat{\rho}^{+}_{R,\mathrm{G}}(t) = (1 - \Delta^2 t^2)\exp(-\Delta^2 t^2/2) \tag{29}$$

$$\hat{\rho}_{1,\mathrm{L}}(t) = \exp(-at) \tag{30}$$

$$\hat{\rho}^{+}_{R,\mathrm{L}}(t) = (1 - at)\exp(-at). \tag{31}$$

We get

$$\hat{\rho}^{+}_{R,\mathrm{GL}}(t) = (1 - \Delta^2 t^2 - at)\exp\left(-\Delta^2 t^2/2\right)\exp(-at) \tag{32}$$

as the oscillation part. Thus, the relaxation function under random directional field distribution is

$$P_{\mathrm{GLKT}}(t) = \frac{1}{3} + \frac{2}{3}(1 - \Delta^2 t^2 - at)\exp\left(-\frac{\Delta^2 t^2}{2} - at\right). \tag{33}$$

This is the correct extension form of the Kubo–Toyabe relaxation function [27,28] for convoluted Gaussian and Lorentzian convolutions. The function becomes Gaussian Kubo–Toyabe if $a = 0$ and Lorentzian Kubo–Toyabe if $\Delta = 0$. The same function was mentioned in Refs. [39,40], although no detailed derivations were shown there.

The behavior of Eq. (33) is shown graphically in Fig. 3 by changing the fraction of the Lorentzian source contribution $f_{\mathrm{L}} = a^2/(\Delta^2 + a^2)$ while keeping $\sqrt{\Delta^2 + a^2} = 1\,\mu\mathrm{s}^{-1}$. One of the most characteristic features of the relaxation function is the dip. The location of the minimum of the dip can be found by taking the derivative of $P_{\mathrm{GLKT}}(t)$ and solving the cubic equation

$$\Delta^4 t^3 + 2a\Delta^2 t^2 + (a^2 - 3\Delta^2)t^2 - 2a = 0. \tag{34}$$

Using Cardano's method, we get the solution

$$t_{\min} = \frac{2}{3}\left[\sqrt{b^2 + 9}\cos(\phi/3) - b\right]/\Delta, \tag{35}$$

where $b = a/\Delta$, and ϕ ($0 \le \phi \le \frac{\pi}{2}$) is chosen so that $\tan\phi = \sqrt{(1 + 9/b^2)^3 - 1}$. Here, the Gaussian and Lorentzian distributions have their minimum dips at $t_{\min} = \sqrt{3}/\Delta$ and $2/a$, respectively.

3. Comparison with other relaxation functions

Several different relaxation functions have been used in an attempt to fit the μSR time spectrum in the crossover regime. Typical trials were to approximate the relaxation as a product of functions of Gaussian and Lorentzian origin. The dip described in Eq. (33) can be compared with several different combinations of the products, as in Fig. 4. Unfortunately, it is obvious that no other function form is successful in reproducing the correct form.

We tested how the SKT function, Eq. (4), can be compared to the exact form. Since there is no equation known relating α and λ to Δ and a, α and λ were just chosen, making the functions the best matched. Figure 5 shows a reasonable match as seen for the case of $f_{\mathrm{L}} = 0.5$. Table 1 shows the fitted α and λ parameters for several mixing ratios. The root-mean-square (RMS) deviation from the

Downloaded from https://academic.oup.com/ptep/article/2021/8/083I01/6335693 by University of Technology, Sydney user on 11 February 2022

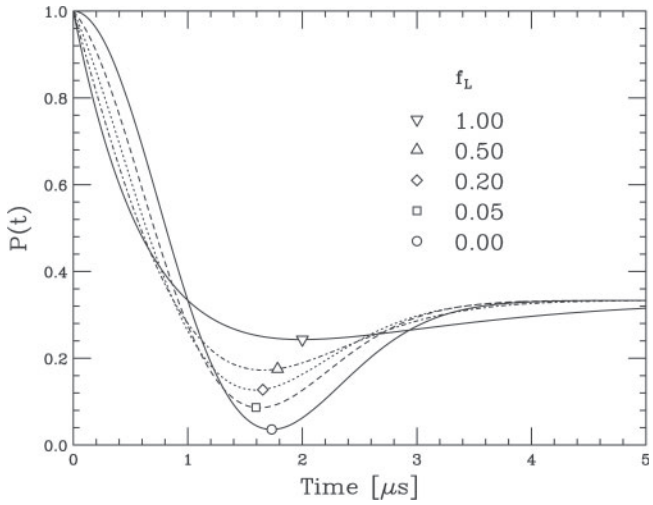

Fig. 3. Simulation of Eq. (33) with different mixing ratios of Lorentzian and Gaussian, $f_{\rm L} = 0$, 0.05, 0.2, 0.5, and 1, while keeping $\sqrt{\Delta^2 + a^2} = 1\,\mu{\rm s}^{-1}$. The locations of the minima are also shown by open marks.

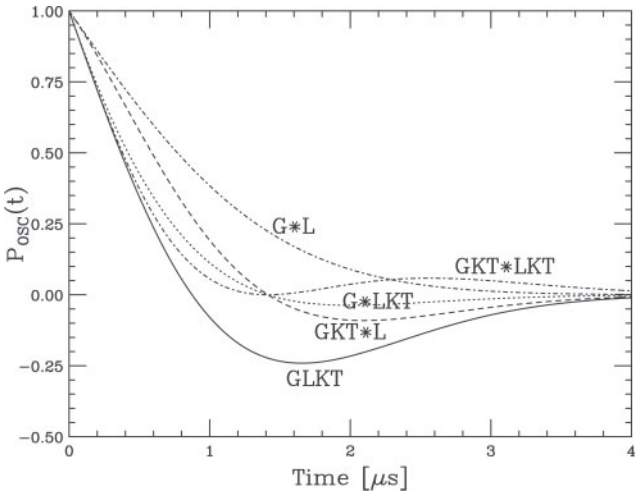

Fig. 4. Comparison of the oscillating part of the relaxation function of Eq. (33) with other functions given as products of relaxation functions of Gaussian and Lorentzian origin with $\Delta = 0.707\,\mu{\rm s}^{-1}$ and $a = 0.707\,\mu{\rm s}^{-1}$, respectively. G: Gaussian, GKT: Gaussian Kubo–Toyabe, L: Lorentzian, LKT: Lorentzian Kubo–Toyabe, and GLKT: extended Kubo–Toyabe functions [Eq. (33)] for the convolution of Gaussian and Lorentzian distributions. G*L: $\exp\left(-\frac{\Delta^2 t^2}{2} - at\right)$, GKT*L: $(1-\Delta^2 t^2)\exp\left(-\frac{\Delta^2 t^2}{2} - at\right)$, G*LKT: $(1-at)\exp\left(-\frac{\Delta^2 t^2}{2} - at\right)$, GKT*LKT: $(1-\Delta^2 t^2)(1-at)\exp\left(-\frac{\Delta^2 t^2}{2} - at\right)$, and GLKT: $(1-\Delta^2 t^2 - at)\exp\left(-\frac{\Delta^2 t^2}{2} - at\right)$.

exact function is also shown. The stretched function parameters seem to reasonably approximate the exact function within the RMS deviation ∼1%. However, some differences are evident such as the slower decrease in $P_{\rm SKT}(t)$ at time zero. Note that the physics basis of the SKT function is vague compared to the exact form.

4. Responses of the intermediate analysis function against external parameters

4.1. Responses to magnetic fields

A μSR experiment in zero-field conditions has the unique and strong advantage of using muons with self-polarization along their initial spin direction. In addition to this, the responses of the μSR time

Downloaded from https://academic.oup.com/ptep/article/2021/8/083I01/6335693 by University of Technology, Sydney user on 11 February 2022

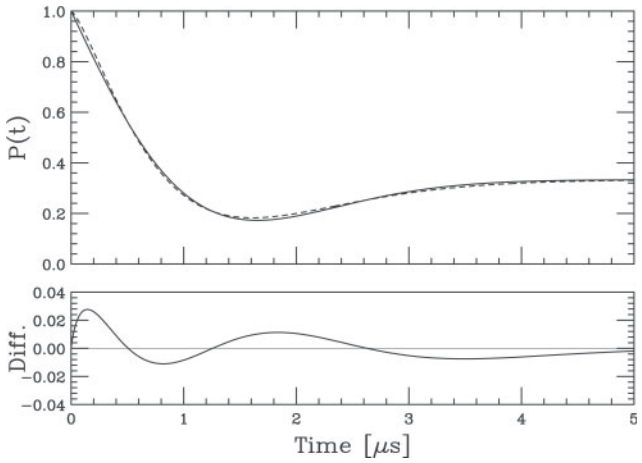

Fig. 5. Top: Comparison of the exact relaxation function Eq. (33) (solid line) and Eq. (4) (dashed line) for $f_L = 0.5$ with $\sqrt{\Delta^2 + a^2} = 1\,\mu s^{-1}$. Bottom: Difference between Eq. (4) and Eq. (33). The best fit was made with $\alpha = 1.315$ and $\lambda = 1.175\,\mu s^{-1}$.

Table 1. Parameters of Eq. (4) given by a fit to Eq. (33). f_L is the mixing ratio of the Lorentzian source; RMS is the root-mean-square discrepancy between the two functions.

Source distribution, $P_{GLKT}(t)$			Stretched Kubo–Toyabe, $P_{SKT}(t)$		
f_L	Δ	a	α_S	λ_S	RMS
0.00	1.0000	0.0000	2.0000	1.0000	0.0000
0.25	0.8660	0.5000	1.4933	1.1791	0.0083
0.50	0.7071	0.7071	1.3146	1.1748	0.0080
0.75	0.5000	0.8660	1.1638	1.1178	0.0059
1.00	0.0000	1.0000	1.0000	1.0000	0.0000

spectrum in magnetic fields applied from outside to materials are also important in investigating the dynamic and static properties of local fields at the muon site [25,26]. In order to investigate the dynamic properties of local fields at the muon site, the magnetic field is applied along the same direction as the initial muon spin polarization. We call this applied magnetic field a longitudinal field (LF). Accordingly, we also created a general formulation to describe the magnetic field dependence of our intermediate analysis function.

In order to describe the LF dependence of the μSR time spectrum, we need to add to the LF the amount of B_0 along the quantum axis, which is the same as the initial muon spin polarization. Since it was not so easy to write down the LF dependence following the same detailed manner as the concept drawn in Fig. 1, we use a different method to derive the final equation. We use the Kubo formula with the Fourier transform of the field distribution [28]:

$$P_z(t, B_0) = 1 - 2t\left(\frac{d}{dt}[Q(t)]\right)\frac{\cos\omega_0 t}{(\omega_0 t)^2} + \frac{2}{\omega_0^2}\lim_{t\to 0}\left(\frac{\frac{d}{dt}[Q(t)]}{t}\right) + 2\int_0^t \frac{\sin\omega_0\tau}{\omega_0^3\tau}\frac{d}{d\tau}\left(\frac{\frac{d}{d\tau}[Q(\tau)]}{\tau}\right)d\tau. \tag{36}$$

Here, $\omega_0 = \gamma_\mu B_0$, and $Q(t)$ is a Fourier transform of the convoluted distribution between Gaussian and Lorentzian. Referencing Eq. (33), $Q(t)$ is given as

$$Q(t) = \exp\left(-at - \frac{\Delta^2 t^2}{2}\right). \tag{37}$$

Downloaded from https://academic.oup.com/ptep/article/2021/8/083I01/6335693 by University of Technology, Sydney user on 11 February 2022

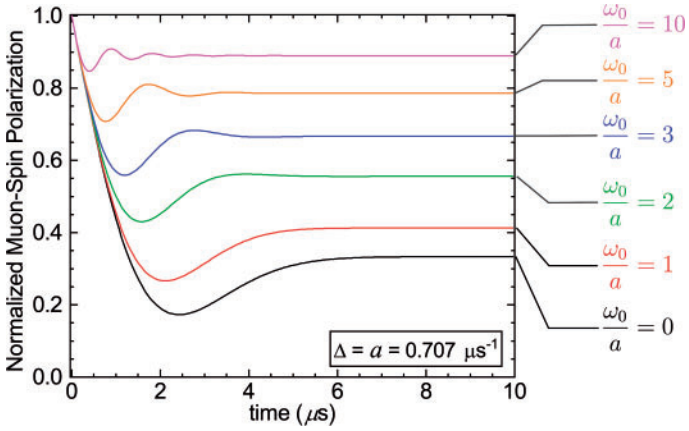

Fig. 6. Equation (33) against variable longitudinal fields with $\Delta = a = 0.707\,\mu s^{-1}$. In the case of $\frac{\omega_0}{a} \gg 10$ the time spectrum is nearly decoupled from the internal field, which has the intermediate distribution between Gaussian and Lorentzian.

Simply calculating this equation, we reach the required equation to describe the LF dependence of the muon spin polarization, $P_{\mathrm{LFGLKT}}(t, B_0)$:

$$\begin{aligned} P_{\mathrm{LFGLKT}}(t,B_0) = 1 &- \frac{a}{\omega_0}\left(J_1(\omega_0 t)\exp\left(-at-\frac{\Delta^2 t^2}{2}\right)\right) \\ &- \frac{2\Delta^2}{\omega_0^2}\left(1-\exp\left(-at-\frac{\Delta^2 t^2}{2}\right)\cos(\omega_0 t)\right) \\ &- \frac{a^2}{\omega_0^2}\left(J_0(\omega_0 t)\exp\left(-at-\frac{\Delta^2 t^2}{2}\right)-1\right) \\ &- \left[1+\left(\frac{a^2-3\Delta^2}{\omega_0^2}\right)\right] a\int_0^t J_0(\omega_0\tau)\exp\left(-a\tau-\frac{\Delta^2\tau^2}{2}\right)d\tau \\ &- \left(\frac{a^2\Delta^2}{\omega_0^2}-\frac{2\Delta^4}{\omega_0^3}\right)\int_0^t \sin(\omega_0\tau)\exp\left(-a\tau-\frac{\Delta^2\tau^2}{2}\right)d\tau \\ &- \frac{a\Delta^2}{\omega_0^2}\int_0^t \cos(\omega_0\tau)\exp\left(-a\tau-\frac{\Delta^2\tau^2}{2}\right)d\tau. \end{aligned} \tag{38}$$

Here, J_0 and J_1 are the zeroth- and first-order spherical Bessel functions, respectively. The other expressions are the same as those used in the previous sections. Figure 6 shows a schematic drawing of Eq. (38) in the case of $\Delta = a = 0.707\,\mu s^{-1}$ with changing LF.

The LF dependence of the time spectrum with increasing LF described by Eq. (38) has similar characteristics to those of the Gaussian and Lorentzian functions [25,26]: (i) the dip in the time spectrum becomes smaller, (ii) the so-called $\frac{1}{3}$-tail of the spectrum goes up, (iii) the additional muon spin precession around LF with the small amplitude appears in an earlier time region, and (iv) the time spectrum becomes almost decoupled from the local fields and locked by the LF keeping the initial muon spin polarization in the case of $\frac{\omega_0}{a} \gg 10$.

Downloaded from https://academic.oup.com/ptep/article/2021/8/083I01/6335693 by University of Technology, Sydney user on 11 February 2022

4.2. Responses to dynamic local fields

In many cases we need to discuss dynamic effects on the μSR time spectrum. Changes in local fields at the muon site in time are caused by magnetic transitions [2–10], molecular dynamics [16], ion/spin diffusions, and muon motion [19–24,29]. If those dynamic changes in local fields happen within the μSR time window (10^{-6}–10^{-11} s), the μSR time spectrum is affected and shows different behavior from the static scenario given in previous sections.

Accordingly, we describe the dynamic effect on the basis of Eq. (33). In order to do this, we need to set some assumptions on the dynamic effect following the well-established methods to take into account the dynamic motion of the muon [26]. These are (i) local fields at the muon site do not change in time, (ii) the muon is hopping in local fields, (iii) the muon's motion can be described as a Markov process with a hopping frequency of ν on the basis of the strong collision model, and (iv) the hopping frequency is within the μSR characteristic time window.

What happens for the muon in these dynamic conditions is as follows. When the muon is trapped at one position at time t, the muon sees static local fields distributed at the muon position and shows Larmor precession motion. The muon does not hop during a short time t' after t and depolarizes its spin polarization following Eq. (33). Just after the muon hops to the next place after t', the muon starts to see different local fields and depolarizes again around those different local fields following Eq. (33) with different initial conditions from those given at t. After the hopping process is repeated within the μSR observation time, which is typically up to around 20 μs in the case of a pulsed muon [42], the final μSR time spectrum, $P_{\mathrm{DGLKT}}(t,\nu)$, can be described as the total sum of those hopping procedures:

$$P_{\mathrm{DGLKT}}(t,\nu) = \exp(-\nu t)\left[P_{\mathrm{GLKT}}(t) + \nu\int_0^t P_{\mathrm{GLKT}}(t-t_1)\,P_{\mathrm{GLKT}}(t_1)\,dt_1 + \nu^2\int_{t_2}^t\int_0^{t_2} P_{\mathrm{GLKT}}(t-t_2)\,P_{\mathrm{GLKT}}(t_2-t_1)\,P_{\mathrm{GLKT}}(t_1)\,dt_2dt_1 + \cdots\right]. \quad (39)$$

Equation (39) is summarized as follows:

$$P_{\mathrm{DGLKT}}(t,\nu) = \exp(-\nu t)\,P_{\mathrm{GLKT}}(t) + \nu\int_0^t \exp\left(-\nu\left(t-t'\right)\right)P_{\mathrm{GLKT}}\left(t-t'\right)P_{\mathrm{DGLKT}}\left(t',\nu\right)dt', \quad (40)$$

where $\exp(-\nu(t-t'))$ is the correlation function of the muon's hopping motion on the basis of the strong collision model [26]. The inverse of ν is related to the dynamic muon spin depolarization rate. This equation has to be solved self-consistently because the right-hand term includes the same depolarization term.

Figure 7 shows a schematic picture of Eq. (40) simulated by changing ν to be 0, 0.2, 0.5, 1, 2, 5, 10, 20, 50, 100, 200, and 500 MHz. Δ and a were set to be some convenient values in order to make the simulated time spectra easy to see within the experimental time region of μSR up to around 10 μs. The overall picture of the response of the μSR time spectrum is different from that described by Eq. (1) (Fig. 7(a) [26]), especially when the ratio $\frac{a}{\Delta}$ becomes large. The $\frac{1}{3}$-tail starts to relax first when the value of ν increases from the zero value. With increasing ν, the dip disappears and the $\frac{1}{3}$-tail can no longer be observed. The time spectrum tends to show no motional narrowing effect for higher values of $\frac{a}{\Delta}$. This is because of the non-negligible LKT component in Eq. (40), which is well known not to show the motional narrowing effect [43–45].

Downloaded from https://academic.oup.com/ptep/article/2021/8/083I01/6335693 by University of Technology, Sydney user on 11 February 2022

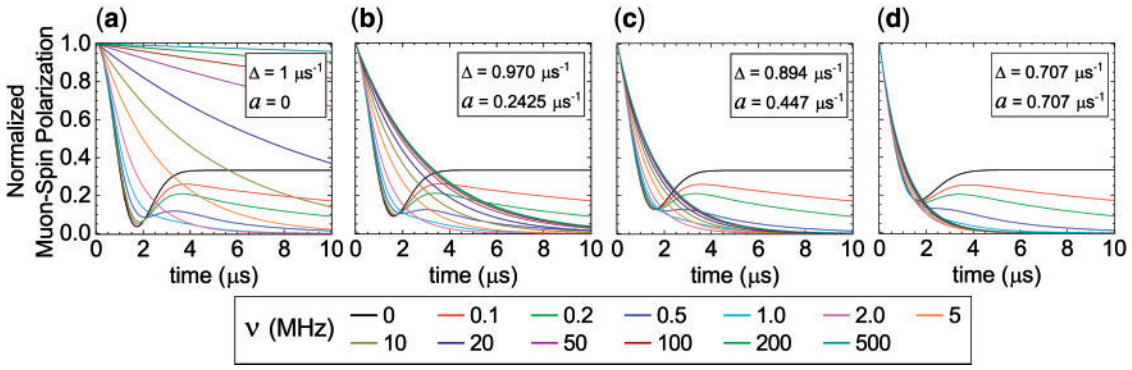

Fig. 7. Schematic picture of Eq. (40) against variable $\nu = 0$, 0.2, 0.5, 1, 2, 5, 10, 20, 50, 100, 200, and 500 MHz. (a) The pure Gaussian case [26]; (b) $\frac{a}{\Delta} = \frac{1}{4}$; (c) $\frac{a}{\Delta} = \frac{1}{2}$; (d) $\frac{a}{\Delta} = 1$. In the case of $\nu \gg 1$ MHz, the time spectrum no longer has the so-called $\frac{1}{3}$-tail.

5. Comparison with μSR data

5.1. Muon spin depolarization by distributed static local fields

Candidate materials to which Eq. (33) may be applied are organic molecules, especially organic molecular superconductors. The general tendency of the crystal structure of these kinds of organic systems shows low-dimensional and anisotropic states. In addition, the atomic components of such organic systems contain only light elements that do not have a large natural abundance of nuclear magnetic moments, like C and O. Those conditions can realize non-uniform and dilute spin conditions.

As an example, the intermediate μSR time spectrum was reported in the paramagnetic state of the low-dimensional organic superconductor λ-$(BETS)_2GaCl_4$ (where BETS = $(CH_2)_2S_2Se_2C_6Se_2S_2(CH_2)_2$) [34]. λ-$(BETS)_2GaCl_4$ shows a superconducting state below about 5.3 K and does not have any clear localized magnetic moment [32–34]. The μSR time spectrum showed the intermediate shape and was independent of temperature in the paramagnetic state [34]. We can technically analyze this intermediate μSR time spectrum by using Eq. (3). However, this method is not necessarily appropriate because almost no localized electronic magnetic moment is expected in this system. From the viewpoint of μSR, the nuclear dipole field is well recognized to be time independent due to the higher frequency of the μSR characteristic time window, which is much faster than dynamic fluctuations of nuclear dipoles [25]. Accordingly, Eq. (33) should be appropriate for analyzing time spectra obtained from μSR measurements on λ-$(BETS)_2GaCl_4$.

We applied Eq. (33) to intermediate μSR time spectra measured in λ-$(BETS)_2GaCl_4$. Figure 8 shows the best-fit results using Eq. (33). The time spectrum was measured at 1 K, 10 K, 20 K, and 50 K, in which the system is in the paramagnetic state and the μSR time spectrum did not show any temperature dependence. The fitting results seem to be very successful, with values of a and Δ of 0.10(1) μs^{-1} and 0.14(1) μs^{-1}, respectively, which indicates that the distribution of local fields at the muon site coming from surrounding nuclear dipoles deviates from Gaussian and becomes the intermediate shape. Since λ-$(BETS)_2GaCl_4$ has an anisotropic low-dimensional crystal structure, there are some spatial regions where the density of nuclear dipoles is largely different. In such a case, some muons which stop near the high- and low-density areas feel stronger and weaker local fields, respectively. This condition makes the field distribution wider and deforms the Gaussian shape.

Downloaded from https://academic.oup.com/ptep/article/2021/8/083I01/6335693 by University of Technology, Sydney user on 11 February 2022

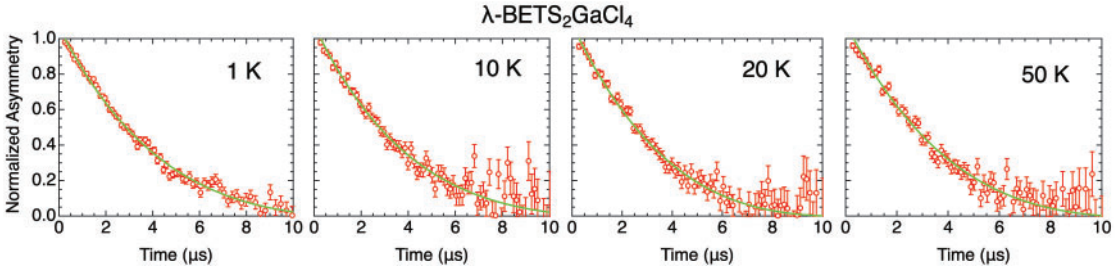

Fig. 8. Time spectra measured for λ-$(BETS)_2GaCl_4$ at 1 K, 10 K, 20 K, and 50 K [34]. The green solid lines indicate the best-fit results using Eq. (33).

5.2. *Muon spin depolarization by fluctuating dynamic local fields*

In addition to the static regime, the dynamic regime due to the appearance of fluctuating dynamic local fields also causes changes in the μSR time spectrum, deforming its shape from Gaussian to the intermediate one as a function of the temperature. An example showing this case was obtained on the La-based high-T_c oxide $La_{2-x}Sr_xCuO_4$ with $x = 0.024$. In this Sr-doping regime, the system was underdoped of carriers and showed the magnetic transition around 10 K. Also, the μSR time spectrum was found to start to divert from Gaussian below 100 K, forming the intermediate shape [36,46]. Our previous study on this system used Eq. (3) in order to discuss changes in the time spectrum on the basis of the appearance of effects of fluctuating dynamic local fields coming from surrounding electronic spins. Although the fitting of time spectra seemed to be good, the possibility of the trading-off effect between λ and Δ could not be removed from the results and discussions. Similar behavior of the μSR time spectrum in the paramagnetic state was also reported in other high-T_c oxides [37,47,48], so that the origin of this change in the μSR time spectrum in the paramagnetic state has been argued to be intrinsic to understanding the mechanism of high-T_c superconductivity [49–51]. However, neither static nor dynamic properties of local magnetic fields which cause tiny changes in the μSR time spectrum are obvious due to the lack of an appropriate intermediate analysis function which can describe the time spectrum between Gaussian and Lorentzian distributions. Following this situation, we applied Eq. (40) to μSR time spectra measured in $La_{2-x}Sr_xCuO_4$ for $x = 0.024$ and tried to reveal the dynamic and static properties of local fields at the muon site. In this case, we can recognize the fluctuating internal field at the muon site as the relative motion against the muon within the scheme of Eq. (40).

Figure 9 shows the fitting results of some of the μSR time spectra observed at about 20 K, 35 K, 50 K, and 100 K in $La_{2-x}Sr_xCuO_4$ for $x = 0.024$. Below 20 K, the temperature was too close to the magnetic transition temperature and the time spectrum becomes nearly the simple exponential type, reflecting that the fluctuating internal field from surrounding electrons became mandatory. As can be seen, the fitting results were successful, proving that Eq. (40) worked well to describe the intermediate state of local fields including fluctuating dynamic components.

Figure 10 displays the temperature dependencies of Δ (left), a (middle), and ν (right). The present analysis using Eq. (40) demonstrates independent properties for each parameter. One new finding was that both Δ and ν increased below around 100 K, where the μSR time spectrum started to deviate from the Gaussian shape, while a remained at almost nothing down to around 20 K. In particular, the temperature dependence of Δ was different from that obtained in our previous results [36]. Therefore, we can finalize that changes below about 100 K in the time spectrum observed in $La_{2-x}Sr_xCuO_4$ for

Downloaded from https://academic.oup.com/ptep/article/2021/8/083I01/6335693 by University of Technology, Sydney user on 11 February 2022

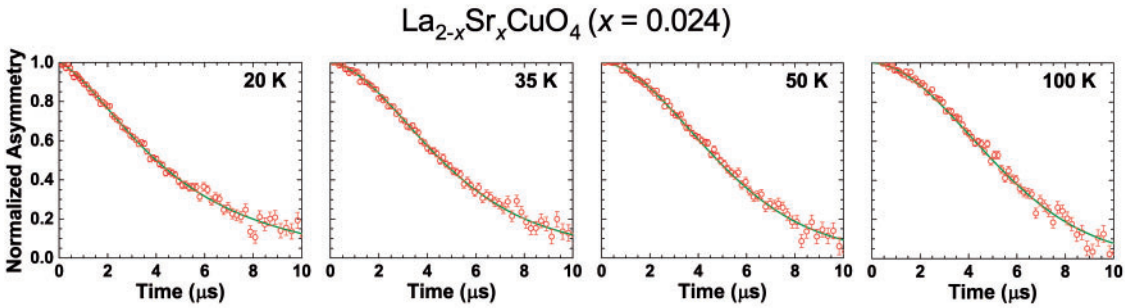

Fig. 9. Analysis results of time spectra measured in $La_{2-x}Sr_xCuO_4$ for $x = 0.024$ at various temperatures. The solid lines in the figure indicate the best-fit results using Eq. (40).

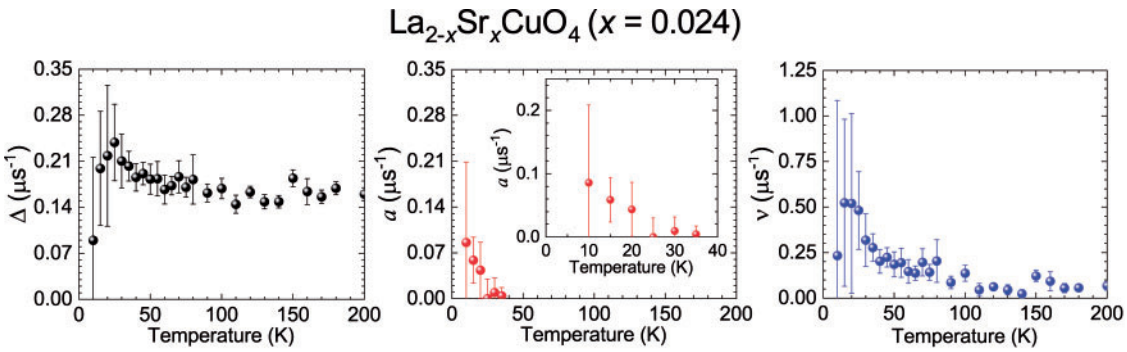

Fig. 10. Temperature dependencies of Δ (left), a (middle), and ν (right) obtained by the application of Eq. (40). The changes in Δ were different from those obtained by applying the phenomenological function of Eq. (3) [36].

$x = 0.024$ are not due to the trading-off effect between Δ and λ, but to the increase of both the width of the static Gaussian distribution and the fluctuating internal fields at the muon site.

6. Summary

We derived μSR relaxation functions under crossover magnetic fields between Gaussian and Lorentzian distributions. We provide a firm basis for matching the relaxation function parameters to the field distribution. The forms of these relaxation functions were found to be a kind of extension of the Kubo–Toyabe relaxation function. We succeeded in describing the relaxation function of the muon spin polarization which was in the intermediate state between Gaussian and Lorentzian in the zero-field and in-field cases.

As demonstrations of our developed analysis equations, we applied them to real μSR data obtained in the organic molecular superconductor λ-$(BETS)_2GaCl_4$ and the La-based high-T_c superconducting cuprates $La_{2-x}Sr_xCuO_4$ for $x = 0.024$, in which the intermediate μSR time spectrum has been observed in the paramagnetic state. We succeeded in reproducing the time spectra using our developed functions. This achievement can correct our previous data obtained from application of the phenomenological function $\exp(-\lambda t) \times P_{GKT}$, which would contain the trading-off effect between two parameters, λ and Δ.

Downloaded from https://academic.oup.com/ptep/article/2021/8/083I01/6335693 by University of Technology, Sydney user on 11 February 2022

The current results and analysis equations described in this report can help to analyze μSR data, and to discuss the physics outlook of the crossover and magnetic transition phenomenon in a clearer manner. As an example, when the zero-field μSR time spectrum deviates from the Gaussian shape in the crossover region and one can analyze the deviation by using Eq. (33), the analysis result indicates the appearance of additional spontaneous internal fields which are comparable to Δ and characterized by a. Furthermore, it is definite that those additional fields are static from the view of the characteristic μSR time window. This analysis method should be worthwhile to quantitatively investigate those spontaneous small internal fields which are expected to result from exotic electronic properties of strongly correlated systems, such as a pseudo gap in the high-T_C superconducting oxides [36,37] and the time reversal symmetry breaking of the superconducting pairing symmetry [11].

Acknowledgements

The authors are grateful to Mr. Muhammad Hanif Che Lah for his cooperative help. This study is supported by the Junior Research Associate (JRA) program of RIKEN and the Japan Society for the Promotion of Science (JSPS) KAKENHI (No. 20H04463).

References

[1] V. W. Hughes and C. S. Wu, *Muon Physics* (Academic Press, New York, 1977).
[2] Y. J. Uemura, J. App. Phys. **64**, 6087 (1988).
[3] J. I. Budnick, A. Golnik, Ch. Niedermayer, E. Recknagel, M. Rossmanith, A. Weidinger, B. Chamberland, M. Filopkowski, and D. P. Yang, Phys. Lett. A **124**, 103 (1987).
[4] T. Kajiwara, I. Watanabe, Y. Kaneko, S. Takaishi, M. Enomoto, N. Kojima, and M. Yamashita, J. Am. Chem. Soc. **129**, 12360 (2007).
[5] T. Ishida, Y. Okamura, and I. Watanabe, Inorg. Chem. **48**, 7012 (2009).
[6] I. Watanabe, T. Adachi, K. Takahashi, S. Yairi, Y. Koike, and K. Nagamine, Phys. Rev. B **65**, 180516(R) (2002).
[7] X. G. Zheng, C. N. Xu, K. Nishikubo, K. Nishiyama, W. Higemoto, W. J. Moon, E. Tanaka, and E. S. Otabe, Phys. Rev. B **72**, 014464 (2005).
[8] G. D. Morris, J. H. Brewer, S. R. Dunsiger, and M. Montour, Hyperfine Inter. **104**, 381 (1997).
[9] P. A. Pattenden, R. M. Valladares, F. L. Pratt, S. J. Blundell, A. J. Fisher, W. Hayes, and T. Sugano, Synth. Met. **71**, 1823 (1995).
[10] V. K. Anand, D. L. Abernathy, D. T. Adroja, A. D. Hillier, P. K. Biswas, and B. Lake, Phys. Rev. B **95**, 224420 (2017).
[11] G. M. Luke et al., Nature **394**, 558 (1998).
[12] A. D. Hillier, J. Quintanilla, and R. Cywinski, Phys. Rev. Lett. **102**, 117007 (2009); **105**, 229901 (2010) [erratum].
[13] Y. J. Uemura et al., Phys. Rev. Lett. **66**, 2665 (1991); **68**, 2712 (1992) [erratum].
[14] A. J. Drew et al., Nature Materials **8**, 310 (2009).
[15] T. Adachi, N. Oki, Risdiana, S. Yairi, Y. Koike, and I. Watanabe, Phys. Rev. B **78**, 134515 (2008).
[16] S. J. Blundell and F. L. Pratt, J. Phys. Condens Matter. **16**, R771 (2004).
[17] I. McKenzie, J. Phys. Chem. B **123**, 4540 (2019).
[18] W. N. Zaharim, H. Rozak, S. Sulaiman, S. N. A. Ahmad, D. F. H. Baseri, S. S. Mohd-Tajudin, A. L. Sin, and I. Watanabe, J. Phys. Soc. Jpn. **90**, 044301 (2021).
[19] K. Nagamine, K. Ishida, T. Matsuzaki, K. Nishiyama, Y. Kuno, T. Yamazaki, and H. Shirakawa, Phys. Rev. Lett. **53**, 1763 (1984).
[20] K. Ishida, K. Nagamine, T. Matsuzaki, Y. Kuno, T. Yamazaki, E. Torikai, H. Shirakawa, and J. H. Brewer, Phys. Rev. Lett. **55**, 2009 (1985).
[21] I. Watanabe, N. Wada, H. Yano, T. Okuno, K. Awaga, S. Ohira, K. Nishiyama, and K. Nagamine, Phys. Rev. B **58**, 2438 (1998).
[22] J. Sugiyama, K. Mukai, Y. Ikedo, H. Nozaki, M. Månsson, and I. Watanabe, Phys. Rev. Lett. **103**, 147601 (2009).
[23] M. Månsson and J. Sugiyama, Phys. Scr. **88**, 068509 (2013).

Downloaded from https://academic.oup.com/ptep/article/2021/8/083I01/6335693 by University of Technology, Sydney user on 11 February 2022

[24] F. L. Pratt, S. J. Blundell, T. Lancaster, C. Baines, and S. Takagi, Phys. Rev. Lett. **96**, 247203 (2006).
[25] R. S. Hayano, Y. J. Uemura, J. Imazato, N. Nishida, T. Yamazaki, and R. Kubo, Phys. Rev. B **20**, 850 (1979).
[26] Y. J. Uemura, T. Yamazaki, D. R. Harshman, M. Senba, and E. J. Ansaldo, Phys. Rev. B **31**, 546 (1985).
[27] R. Kubo and T. Toyabe, in *Magnetic Resonance and Relaxation*, ed. R. Blinc (North Holland, Amsterdam, 1967).
[28] R. Kubo, Hyperfine Interact. **8**, 731 (1981).
[29] R. Kadono, J. Imazato, T. Matsuzaki, K. Nishiyama, K. Nagamine, T. Yamazaki, D. Richter, and J.-M. Welter, Phys. Rev. B **39**, 23 (1989).
[30] I. Watanabe, T. Adachi, S. Yairi, Y. Koike, and K. Nagamine, J. Phys. Soc. Jpn **77**, 124716 (2008).
[31] R. E. Walstedt and L. R. Walker, Phys. Rev. **9**, 4857 (1974).
[32] S. Imajo, N. Kanda, S. Yamashita, H. Akutsu, Y. Nakazawa, H. Kumagai, T. Kobayashi, and A. Kawamoto, J. Phys. Soc. Jpn. **85**, 043705 (2016).
[33] T. Kobayashi, H. Taniguchi, A. Ohnuma, and A. Kawamoto, Phys. Rev. B **102**, 121106(R) (2020).
[34] D. P. Sari et al., IOP Conf. Ser. Mat. Sci. Eng. **196**, 012047 (2017).
[35] V. K. Anand, D. L. Abernathy, D. T. Adroja, A. D. Hillier, P. K. Biswas, and B. Lake, Phys. Rev. B **95**, 224420 (2017).
[36] I. Watanabe, T. Adachi, S. Yairi, Y. Koike, and K. Naganime, J. Phy. Soc. Jpn. **77**, 124716 (2008).
[37] C. Panagopoulos, J. L. Tallon, B. D. Rainford, T. Xiang, J. R. Cooper, and C. A. Scott, Phys. Rev. B **66**, 064501 (2002).
[38] M. R. Crook and R. Cywinski, J. Phys.: Condens Matter. **9**, 1149 (1997).
[39] A. Maisuradze, W. Schnelle, R. Khasanov, R. Gumeniuk, M. Nicklas, H. Rosner, A. Leithe-Jasper, Yu. Grin, A. Amato, and P. Thalmeier, Phys. Rev. B **82**, 024524 (2010).
[40] J. S. Lord, J. Phys.: Conf. Ser. **17**, 014 (2005).
[41] H. Takahashi and Y. Tanimura, J. Phys. Soc. Jpn. **89**, 064710 (2020).
[42] K. Nagamine, T. Matsuzaki, K. Ishida, I. Watanabe, R. Kadono, G. H. Eaton, H. J. Jones, G. Thomas, and W. G. Williams, Hyperfine Interact. **87**, 1091 (1994).
[43] A. T. Fiory, Hyperfine Interact. **8**, 777 (1981).
[44] M. Leon, Hyperfine Interact. **8**, 781 (1981).
[45] R. H. Silsbee and D. W. Hone, Phys. Rev. B **27**, 85 (1983).
[46] I. Watanabe, J. Phy. Soc. Jpn. **63**, 1560 (1994).
[47] J. E. Sonier et al., Science **292**, 1692 (2001).
[48] J. E. Sonier et al., Phys. Rev. B **66**, 134501 (2002).
[49] C. M. Varma, Phys. Rev. B **73**, 155113 (2006).
[50] B. Fauqué, Y. Sidis, V. Hinkov, S. Pailhès, C. T. Lin, X. Chaud, and P. Bourges, Phys. Rev. Lett. **96**, 197001 (2006).
[51] J. Xia et al., Phys. Rev. Lett. **100**, 127002 (2008).

Downloaded from https://academic.oup.com/ptep/article/2021/8/083I01/6335693 by University of Technology, Sydney user on 11 February 2022